Supplemental Material for "Athermal fluctuations in disordered crystals"

Pappu Acharya,[1,*] Surajit Sengupta,[1,†] Bulbul Chakraborty,[2,‡] and Kabir Ramola[1,§]

[1] *Centre for Interdisciplinary Sciences, Tata Institute of Fundamental Research, Hyderabad 500107, India*
[2] *Martin Fisher School of Physics, Brandeis University, Waltham, MA 02454, USA*

In this document we provide supplemental figures and details related to the results presented in the main text.

I. SIMULATING THERMAL DISORDER

In this section we study thermal crystals using finite temperature Monte Carlo simulations. We simulate two distinct systems (i) a crystal of equal sized particles governed by a force law (Eq. (2) in the main text), and (ii) a crystal with forces not related to the inter-particle distances, but force balanced at all times. In the latter case we posit a quadratic Hamiltonian governing the forces that couples to the temperature of the system. In both cases we observe Gaussian fluctuations of the forces along all directions, showing that the constrained fluctuations observed in athermal systems arise from both local force balance conditions *and* the force law relating the positions to the forces in the system.

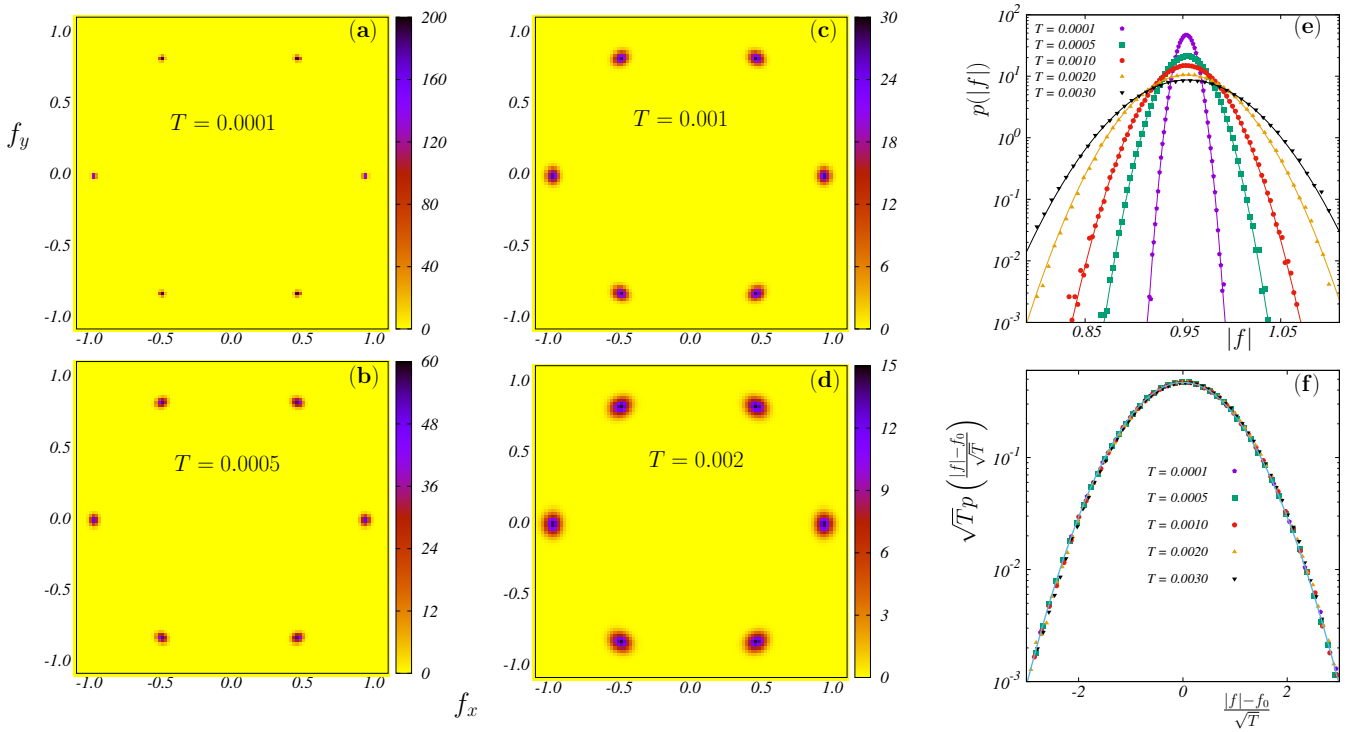

FIG. 1: **(a) - (d)** Two dimensional distributions $p(f_x, f_y)$ of the forces $\vec{f} \equiv (f_x, f_y)$ in the system at different temperatures obtained from Monte Carlo simulations of thermal crystals. The fluctuations about the crystalline values are Gaussian with a width $\propto \sqrt{T}$, exhibiting thermal broadening along the lattice directions as well as directions perpendicular to the lattice. **(e)** The distributions of the magnitudes of the forces $p(|f|)$ are Gaussian at all simulated temperatures, the bold lines represent best-fit Gaussians. **(f)** These distributions can be collapsed with the single scaling variable $\zeta = (|f| - f_0)/\sqrt{T}$.

*Electronic address: pappuacharya@tifrh.res.in
†Electronic address: surajit@tifrh.res.in
‡Electronic address: bulbul@brandeis.edu
§Electronic address: kramola@tifrh.res.in

A. Thermal Crystal

In our simulations of thermal crystals, the interactions between particles is modeled with the one-sided harmonic law given in Eq. (1) in the main text. All particles have equal radii with $\sigma_i = \sigma_0 = \frac{1}{2}$, forming a triangular lattice at $T = 0$. At finite temperatures, we allow fluctuations in the particle positions of magnitude $\propto \sqrt{T}$, and use Metropolis sampling to accept or reject configurations. It should be noted that the states sampled by these simulations violate the local force balance conditions at every time, since the system is not at an energy minimum. The two dimensional distributions of the forces obtained from these simulations is plotted in Fig. 1 **(a)** - **(d)**. At $T = 0$ the distribution is peaked at six locations governed by the crystalline angles with magnitude f_0 (Eq. (4) in the main text). These peaks spread as the temperature increases, exhibiting Gaussian fluctuations in both $f_\perp$ and $f_{||}$ (shown in Fig. 2 **(b)** in the main text). Consequently the distribution of the magnitude of the forces $|f|$ also displays Gaussian fluctuations as displayed in Fig. 1 **(e)**. These distributions can be collapsed with the scaling variable $\zeta = (|f| - f_0)/\sqrt{T}$ as shown in Fig. 1 **(f)**.

B. "Thermal" force balanced crystal

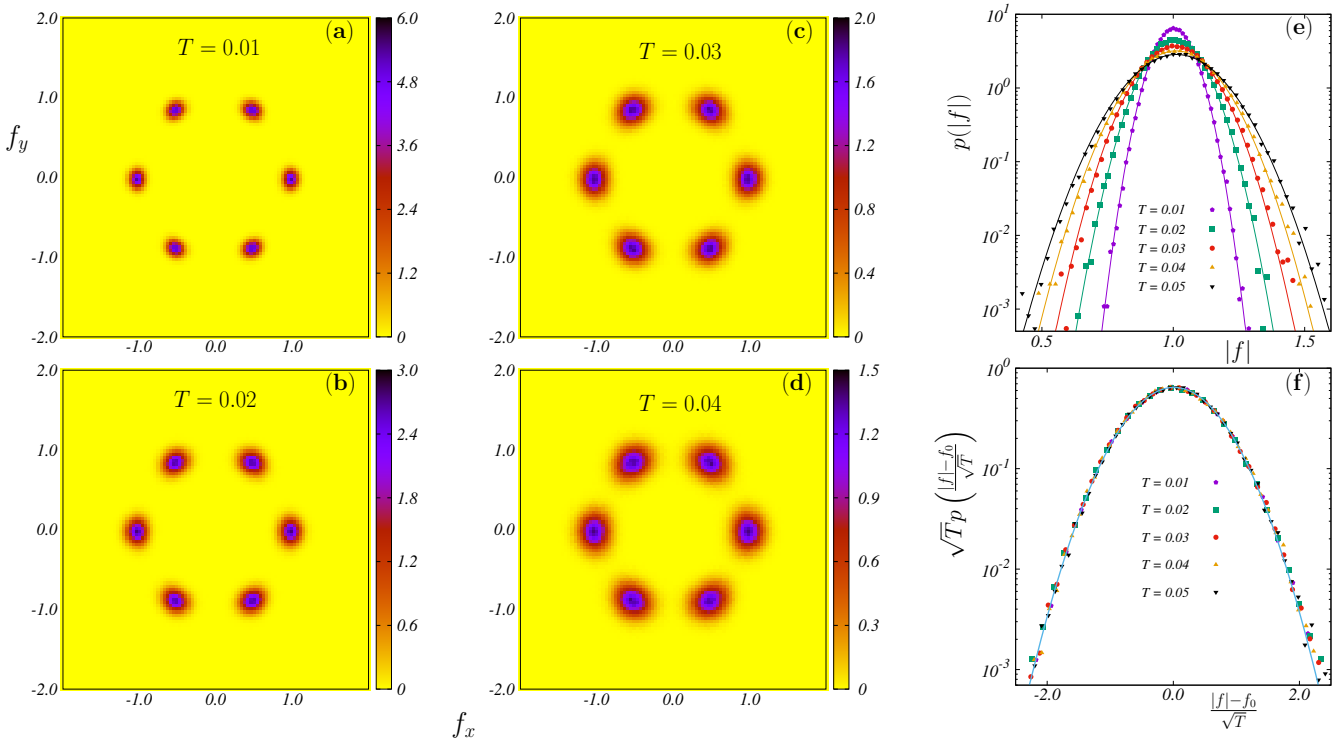

FIG. 2: **(a)** - **(d)** Two dimensional distributions $p(f_x, f_y)$ of the forces $\vec{f} \equiv (f_x, f_y)$ in the system at different temperatures obtained from Monte Carlo simulations of crystals in force balance without a force law. The fluctuations about the crystalline values are Gaussian with a width $\propto \sqrt{T}$, once again exhibiting thermal broadening along both the lattice directions as well as directions perpendicular to the lattice. **(e)** The distributions of the magnitudes of the forces $p(|f|)$ are Gaussian at all simulated temperatures, the bold lines represent best-fit Gaussians. **(f)** These distributions can be collapsed with the single scaling variable $\zeta = (|f| - f_0)/\sqrt{T}$.

Since constrained fluctuations arising in athermal systems originate from local force balance conditions, it is interesting to ask whether such fluctuations can be obtained from an effective Hamiltonian *with force balance* on every particle. We therefore postulate an effective Hamiltonian of the harmonic form

$$H = \epsilon_f \sum_{\langle ij \rangle} \left(\vec{f}_{ij} - \vec{f}^0_{ij} \right)^2 . \tag{1}$$

Here $\vec{f}_{ij}^{0}$ are the value of the forces in the pure crystal ($\eta = 0$). In our simulations we set the stiffness $\epsilon_f = 1$. Since we also incorporate the force balance constraint on every grain

$$\sum_j \vec{f_{ij}} = 0, \tag{2}$$

the finite temperature partition function of such a system is given by

$$Z(\beta) = \int \prod_{ij} d\vec{f}_{ij} \prod_i \delta \left(\sum_j \vec{f_{ij}} \right) \exp\left(-\beta H\right), \tag{3}$$

where $\beta = 1/T$ is the inverse temperature. We note that since the position degrees of freedom are absent in the above formalism, this represents a system in force balance, but with forces not originating from an underlying force law such as Eq. (2) in the main text. In order to incorporate the local force balance constraints, we parameterize the forces in the system in terms of auxiliary fields placed on the voids between grains, termed "height fields" [1, 2]. We then perform Monte Carlo simulations by allowing fluctuations in these height fields of magnitude $\propto \sqrt{T}$, and use Metropolis sampling to accept or reject configurations with the Hamiltonian in Eq. (1). Results from these simulations are presented in Fig. 2. We find that this system exhibits properties identical to a thermal crystal without force balance (with an underlying force law). We therefore conclude that the constrained fluctuations exhibited by athermal systems originate from the local force balance conditions imposed on the *positions* that yield the forces in the system. This is precisely what the disorder perturbation expansion developed in the main text accomplishes.

II. SIMULATING ATHERMAL DISORDER

Our simulation of athermal disorder follows a standard technique for creating jammed packings of frictionless disks. We begin with a triangular lattice arrangement of the particles, with all radii equal ($\sigma_0 = 1/2$). We then change the particle radii as mentioned in Eq. (6) in the main text. Finally, we rescale all the radii to keep the packing fraction intact (see Section II A). In order to minimize the energy of the system we use the FIRE (Fast Inertial Relaxation Engine) algorithm [3], followed by a molecular dynamics update. FIRE is simple to incorporate and rapidly leads to a minimum energy configuration. In our implementation we compute the power $P = \vec{F}.\vec{v}$ in the entire system at every time step. If $P > 0$, the velocity is set to $\vec{v} \to (1-\beta)\vec{v} + \beta\hat{F}|\vec{v}|$, the time step is increased as $\Delta t = \Delta t f_{\rm inc}$ upto a maximum value $\Delta t = \Delta t_{\rm max}$ and β is changed to βf_β. However if $P < 0$, the velocity is set to zero, the time step is decreased as $\Delta t = \Delta t f_{\rm dec}$ and β is reset back to its initial value $\beta_{\rm start}$. After each such step, we return to the molecular dynamics simulations and update the system with the new velocities. We repeat this process until a desired threshold for force balance in our system is achieved. In our simulations we set $\beta = \beta_{\rm start} = 0.01$, $\Delta t = 0.0001$, $\Delta t_{\rm max} = 0.001$, $f_\beta = 0.99$, $f_{\rm inc} = 1.1$, and $f_{\rm dec} = 0.5$.

A. Boundary Conditions

In our simulation of athermal disorder, we work in a fixed packing fraction ensemble (similar to Ref. [4]). The athermal perturbation, due to the change in particle radii, changes the packing fraction of the system. Therefore, in our simulations, for a given realization of the disorder (i.e. incremental sizes of the particles), we rescale the radii of all particles (by the same factor) in order to maintain a fixed packing fraction. Note that this rescaling does not affect the force distributions to *linear order*, as we show below. The packing fraction ϕ is determined through the equation

$$\phi = \frac{1}{V} \sum_{i=1}^{N} \pi \sigma_i^2, \tag{4}$$

where $V = L_x L_y$ is the volume of the system. The addition of athermal disorder changes the radii as $\sigma_i \to \sigma_0(1+\eta x_i)$, with x_i drawn from a uniform distribution in the interval $\left[-\frac{1}{2}, \frac{1}{2}\right]$. This leads to the following expansion for the packing fraction

$$\phi' = \phi^0 + \frac{\sum_{i=1}^{N} \eta^2 x_i^2}{V} = \phi^0 + \frac{\eta^2}{48V} + \mathcal{O}(\eta^3), \tag{5}$$

where ϕ^0 is the packing fraction of the unperturbed crystal, and since $\sum_{i=1}^{N} \eta x_i \to 0$ for large N. Hence, the effect of the rescaling only contributes at order η^2. Similarly, the generalized expression for the force in the pure crystal (Eq. (14)) is not affected by the rescaling to leading order. Finally, we have also checked that the force distributions we obtain do not differ before and after rescaling to linear order.

III. PARALLEL AND PERPENDICULAR FORCE COMPONENTS

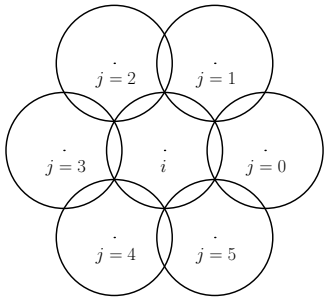

FIG. 3: The labeling convention. The six neighbours of every particle i are labeled as $j = 0$ to 5. The bond angles between these particles can take any of six values (depending on i and j) with the positive x-axis, $\theta^0_{ij} = 0$, $\pi/3$, $2\pi/3$, π, $4\pi/3$, and $5\pi/3$.

For a perfect crystal (i.e. no disorder) every particle i has six neighbours j. The bond angles between these particles can take any of six values (depending on i and j) with the positive x-axis, $\theta^0_{ij} = 0$, $\pi/3$, $2\pi/3$, π, $4\pi/3$, and $5\pi/3$. In the main text, we have termed these six directions the 'lattice directions'. The directions orthogonal to these six directions are termed the perpendicular (or orthogonal) directions. In the pure crystal, the forces lie precisely along the lattice directions. However, when disorder is introduced, the positions of the particles shift, leading to a finite component along the orthogonal directions. We define these components with respect to the *original* lattice directions as

$$\begin{aligned} f_{\parallel} &= |f_{ij}| \cos(\theta_{ij} - \theta^0_{ij}), \\ f_{\perp} &= |f_{ij}| \sin(\theta_{ij} - \theta^0_{ij}). \end{aligned} \tag{6}$$

Here $|f_{ij}|$ is the magnitude of the force between particles i and j in the disordered ground state. Therefore, in effect we are resolving the perturbed forces along the original crystal structure. Remarkably, this resolution of the forces uncovers a sharp distinction between thermal and athermal crystals, as we show in our study.

IV. FORCES IN THE PURE CRYSTAL

In this section we relate the magnitude of the force f_0 in a pure crystal ($\eta = 0$) to the packing fraction ϕ. Since we set the radius of every particle in the crystalline state to σ_0, the linear dimensions $L_y = \frac{\sqrt{3}}{2} L_x$ of the system are determined by the packing fraction ϕ through the equation

$$\phi = \frac{N\pi\sigma_0^2}{\frac{\sqrt{3}}{2} L_x^2}. \tag{7}$$

For a fixed L_x, this leads to the relation

$$\frac{\phi}{\phi_c} = \frac{\sigma_0^2}{\sigma_{0,c}^2}, \tag{8}$$

where ϕ_c and $\sigma_{0,c}$ are the packing fraction and radii of particles in the marginal crystal (with no overlaps between particles) respectively. As the system is in a triangular lattice arrangement of $\sqrt{N} \times \sqrt{N}$ particles, L_x can be related

to the overlap Δr between the particles as

$$L_x = \sqrt{N}(2\sigma_0 - \Delta r). \tag{9}$$

Therefore

$$\Delta r = 2\sigma_0 - \frac{L_x}{\sqrt{N}}. \tag{10}$$

Next, we can use this to determine the radii of the particles in the marginal crystal by setting $\Delta r = 0$, yielding

$$\sigma_{0,c}^2 = \frac{L_x^2}{4N}. \tag{11}$$

We note that inserting this value into Eq. (7) yields the packing fraction for the hexagonal close packed structure $\phi_c = \frac{\pi}{\sqrt{12}}$. We next relate the overlaps between particles to the inter-particle forces. Combining Eqs. (8), (10) and (11), we have

$$\Delta r = 2\sigma_0 \left(1 - \sqrt{\frac{\phi_c}{\phi}}\right). \tag{12}$$

Setting $\epsilon = 1$ in the force law in Eq. (2) in the main text, we have

$$f_0 = \frac{1}{2\sigma_0}\left(\frac{\Delta r}{2\sigma_0}\right). \tag{13}$$

Using the expression for the overlap in Eq. (12) in the above expression, we arrive at

$$f_0 = \frac{1}{2\sigma_0}\left(1 - \sqrt{\frac{\phi_c}{\phi}}\right). \tag{14}$$

Finally, setting the value $\sigma_0 = \frac{1}{2}$ (as in our simulations), we have

$$f_0 = 1 - \sqrt{\frac{\phi_c}{\phi}}, \tag{15}$$

which is Eq. (5) in the main text.

V. LINEARIZED FORCE BALANCE EQUATIONS

In this section we provide details of the disorder perturbation expansion developed in the main text. The general form of the interaction between particles is given by

$$\begin{aligned} V_{\sigma_{ij}}(\vec{r}_{ij}) &= \frac{\epsilon}{\alpha}\left(1 - \frac{|\vec{r}_{ij}|}{\sigma_{ij}}\right)^{\alpha} \quad \text{for} \quad r_{ij} < \sigma_{ij}, \\ &= 0 \qquad\qquad\qquad\quad \text{for} \quad r_{ij} \geq \sigma_{ij}. \end{aligned} \tag{16}$$

The forces in the system are determined by the inter-particle distances as

$$\vec{f}_{ij} = \frac{\epsilon}{\sigma_{ij}}\left(1 - \frac{|r_{ij}|}{\sigma_{ij}}\right)^{\alpha-1} \hat{r}_{ij}. \tag{17}$$

The two components of the forces can be expressed as

$$f_{ij}^x = \frac{\epsilon}{\sigma_{ij}}\left(1-\frac{\sqrt{x_{ij}^2+y_{ij}^2}}{\sigma_{ij}}\right)^{\alpha-1}\frac{x_{ij}}{\sqrt{x_{ij}^2+y_{ij}^2}},$$
$$f_{ij}^y = \frac{\epsilon}{\sigma_{ij}}\left(1-\frac{\sqrt{x_{ij}^2+y_{ij}^2}}{\sigma_{ij}}\right)^{\alpha-1}\frac{y_{ij}}{\sqrt{x_{ij}^2+y_{ij}^2}}. \quad (18)$$

We note that these equations are non-linear in the components x_{ij} and y_{ij}. We next treat the polydispersity as a perturbation, with

$$\sigma_i = \sigma_0 + \delta\sigma_i. \quad (19)$$

As a response to this perturbation from the crystalline state, the positions of the particles also change as

$$\begin{aligned} x_i &= x_{i,0} + \delta x_i, \\ y_i &= y_{i,0} + \delta y_i. \end{aligned} \quad (20)$$

Expanding Eq. (18) to linear order in δx_i and δy_i, the change in the forces due to the disorder can be expressed as

$$\begin{aligned} \delta f_{ij}^x &= C_{ij}^{xx}\delta x_{ij} + C_{ij}^{xy}\delta y_{ij} + C_{ij}^{x\sigma}\delta\sigma_{ij}, \\ \delta f_{ij}^y &= C_{ij}^{yx}\delta x_{ij} + C_{ij}^{yy}\delta y_{ij} + C_{ij}^{y\sigma}\delta\sigma_{ij}, \end{aligned} \quad (21)$$

where the coefficients $C_{ij}^{\beta\gamma}(\phi)$ only depend on the packing fraction ϕ. These coefficients are translationally invariant, i.e. they do not depend on the particle index i. We compute them for a particle i, with the neighbouring particles labeled $j = 0$ to 5 (see Fig. 3). The coefficients can then be expressed as (setting $\epsilon = 1$)

$$\begin{aligned} C_{ij}^{xx}(\phi) &= -\frac{\left(1-\sqrt{\frac{\phi_c}{\phi}}\right)^{\alpha-2}\left(\alpha\sqrt{\frac{\phi_c}{\phi}}+\cos\left(\frac{2\pi j}{3}\right)\left((\alpha-2)\sqrt{\frac{\phi_c}{\phi}}+1\right)-1\right)}{2\sqrt{\frac{\phi_c}{\phi}}}, \\ C_{ij}^{xy}(\phi) &= -\frac{\sin\left(\frac{2\pi j}{3}\right)\left(1-\sqrt{\frac{\phi_c}{\phi}}\right)^{\alpha-2}\left((\alpha-2)\sqrt{\frac{\phi_c}{\phi}}+1\right)}{2\sqrt{\frac{\phi_c}{\phi}}}, \\ C_{ij}^{x\sigma}(\phi) &= \cos\left(\frac{\pi j}{3}\right)\left(1-\sqrt{\frac{\phi_c}{\phi}}\right)^{\alpha-2}\left(\alpha\sqrt{\frac{\phi_c}{\phi}}-1\right), \\ C_{ij}^{yy}(\phi) &= \frac{\left(1-\sqrt{\frac{\phi_c}{\phi}}\right)^{\alpha-2}\left(\alpha\left(-\sqrt{\frac{\phi_c}{\phi}}\right)+\cos\left(\frac{2\pi j}{3}\right)\left((\alpha-2)\sqrt{\frac{\phi_c}{\phi}}+1\right)+1\right)}{2\sqrt{\frac{\phi_c}{\phi}}}, \\ C_{ij}^{yx}(\phi) &= -\frac{\sin\left(\frac{2\pi j}{3}\right)\left(1-\sqrt{\frac{\phi_c}{\phi}}\right)^{\alpha-2}\left((\alpha-2)\sqrt{\frac{\phi_c}{\phi}}+1\right)}{2\sqrt{\frac{\phi_c}{\phi}}}, \\ C_{ij}^{y\sigma}(\phi) &= \sin\left(\frac{\pi j}{3}\right)\left(1-\sqrt{\frac{\phi_c}{\phi}}\right)^{\alpha-2}\left(\alpha\sqrt{\frac{\phi_c}{\phi}}-1\right), \end{aligned} \quad (22)$$

where $\phi_c = \pi/\sqrt{12}$ is the packing fraction of the marginal crystal (with zero overlaps).

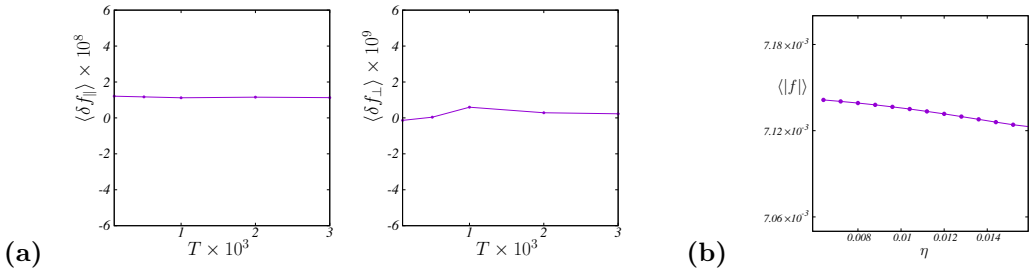

FIG. 4: The change in the mean value of the forces with increasing disorder strength for **(a)** thermal and **(b)** athermal systems. The scale has been magnified to show the effect of the small non-linear behaviour in the region of interest of our present study.

A. Coefficients for harmonic interactions

For the harmonic case ($\alpha = 2$) that we study using simulations, the coefficients in the linearized force balance expansion have a particularly simple form, given by

$$\begin{aligned}
C_{ij}^{xx}(\phi) &= \frac{\sin^2\left(\frac{\pi j}{3}\right)}{\sqrt{\phi_c/\phi}} - 1, \\
C_{ij}^{xy}(\phi) &= -\frac{\sin\left(\frac{\pi j}{3}\right)\cos\left(\frac{\pi j}{3}\right)}{\sqrt{\phi_c/\phi}}, \\
C_{ij}^{x\sigma}(\phi) &= \left(2 - \frac{1}{\sqrt{\phi_c/\phi}}\right)\sqrt{\phi_c/\phi}\cos\left(\frac{\pi j}{3}\right), \\
C_{ij}^{yy}(\phi) &= \frac{\cos^2\left(\frac{\pi j}{3}\right)}{\sqrt{\phi_c/\phi}} - 1, \\
C_{ij}^{yx}(\phi) &= -\frac{\sin\left(\frac{\pi j}{3}\right)\cos\left(\frac{\pi j}{3}\right)}{\sqrt{\phi_c/\phi}}, \\
C_{ij}^{y\sigma}(\phi) &= \left(2 - \frac{1}{\sqrt{\phi_c/\phi}}\right)\sqrt{\phi_c/\phi}\sin\left(\frac{\pi j}{3}\right).
\end{aligned} \tag{23}$$

VI. MEAN VALUE OF FORCES

In this section we describe the variation in the mean value of the forces, with the introduction of both thermal and athermal disorder.

A. Thermal Disorder

For small disorder, the distributions are symmetric about their average values, and the mean values of these fluctuations are $\langle \delta f_\parallel \rangle = 0$ and $\langle \delta f_\perp \rangle = 0$. This is true if one considers the linear response of the total energy of the system to the transformation $\delta f_{ij}^{x(y)} \to -\delta f_{ij}^{x(y)}$. This transformation leaves the Hamiltonian of the system invariant, to linear order. Similarly, the transformation leaves the Hamiltonian of the thermal force balanced crystal (Eq. (1)) invariant. Hence at low temperatures, where the linear regime dominates, the mean value of the forces remains constant. In Fig. 4 (a) we plot the variation of the mean value of the force in the thermal system obtained in our simulations, highlighting the almost constant behaviour as the temperature is varied.

B. Athermal Disorder

Within the linear theory, the mean value f_0 is independent of the polydispersity, as the mean positions of the particles are the crystalline positions of the original triangular lattice. However, there could be non-trivial corrections

to this behaviour with increasing disorder. This is however a higher order effect, since in the linear theory the forces are completely determined by a *linear* "Green's function" connecting the displacements to the disorder in the radii (Eq. (9) in the main text). Hence, for a given realization of the athermal disorder, the transformation $\{\eta_i\} \to \{-\eta_i\}$ transforms the force deviations as $\delta f_{ij}^{x(y)} \to -\delta f_{ij}^{x(y)}$. Hence to linear order, the force fluctuations are symmetric about their mean value. In Fig. 4 (b) we plot the variation of the mean value of the force in the system obtained in our simulations, highlighting the small variation as the strength of the athermal disorder is increased.

VII. FOURIER SPACE REPRESENTATION

Following the convention in Fig. 3, the force balance on every grain i can be expressed as

$$\vec{f}_{i0} + \vec{f}_{i1} + \vec{f}_{i2} + \vec{f}_{i3} + \vec{f}_{i4} + \vec{f}_{i5} = 0. \tag{24}$$

Using the linearized expressions in Eq. (21) this leads to equations relating the changes in the positions to the changes in the radii as

$$\begin{aligned}
\sum_{j=0}^{5} C_{ij}^{xx}(\delta x_i - \delta x_j) + \sum_{j=0}^{5} C_{ij}^{xy}(\delta y_i - \delta y_j) &= -\sum_{j=0}^{5} C_{ij}^{x\sigma}(\delta\sigma_i + \delta\sigma_j), \\
\sum_{j=0}^{5} C_{ij}^{yx}(\delta x_i - \delta x_j) + \sum_{j=0}^{5} C_{ij}^{yy}(\delta y_i - \delta y_j) &= -\sum_{j=0}^{5} C_{ij}^{y\sigma}(\delta\sigma_i + \delta\sigma_j).
\end{aligned} \tag{25}$$

Next, we define the Fourier transforms of the changes in positions and radii as

$$\begin{aligned}
\delta x(\vec{k}) &= \sum_{\vec{r}} \exp(i\vec{k}.\vec{r})\delta x(\vec{r}), \\
\delta y(\vec{k}) &= \sum_{\vec{r}} \exp(i\vec{k}.\vec{r})\delta y(\vec{r}), \\
\delta\sigma(\vec{k}) &= \sum_{\vec{r}} \exp(i\vec{k}.\vec{r})\delta\sigma(\vec{r}).
\end{aligned} \tag{26}$$

Here $\vec{r} \equiv i$ label the sites of the triangular lattice whereas

$$\vec{k} \equiv (k_x, k_y) \equiv \left(\frac{2\pi l}{2N}, \frac{2\pi m}{N}\right), \tag{27}$$

are the reciprocal lattice vectors of the triangular lattice [5]. Since the changes in the radii are i.i.d. variables, we have (using Eq. (6) in the main text)

$$\langle \delta\sigma(\vec{r})\delta\sigma(\vec{r'})\rangle = \eta^2\sigma_0^2\delta(\vec{r} - \vec{r'}) \int_{-1/2}^{1/2} d\xi\ \xi^2 = \frac{\eta^2}{48}\delta(\vec{r} - \vec{r'}), \tag{28}$$

where we have used $\sigma_0 = 1/2$. This can then be used to compute the correlations in Fourier space as

$$\langle \delta\sigma(\vec{k})\delta\sigma(-\vec{k})\rangle = \frac{\eta^2}{48}. \tag{29}$$

It is also convenient to define the following Fourier coefficients

$$\begin{aligned}
\mathcal{F}_0(\vec{k}) &= e^{-2ik_x}, \\
\mathcal{F}_1(\vec{k}) &= e^{-ik_x - ik_y}, \\
\mathcal{F}_2(\vec{k}) &= e^{ik_x - ik_y}, \\
\mathcal{F}_3(\vec{k}) &= e^{2ik_x}, \\
\mathcal{F}_4(\vec{k}) &= e^{ik_x + ik_y}, \\
\mathcal{F}_5(\vec{k}) &= e^{ik_y - ik_x}.
\end{aligned} \tag{30}$$

Next, multiplying Eq. (25) by $\exp(i\vec{k}.\vec{r})$ and summing over all sites $\vec{r} \equiv i$ leads to the following matrix equation at every $\vec{k}$

$$\begin{pmatrix} A^{xx}(\vec{k}) & A^{xy}(\vec{k}) \\ A^{yx}(\vec{k}) & A^{yy}(\vec{k}) \end{pmatrix} \begin{pmatrix} \delta x(\vec{k}) \\ \delta y(\vec{k}) \end{pmatrix} = \delta\sigma(\vec{k}) \begin{pmatrix} D^x(\vec{k}) \\ D^y(\vec{k}) \end{pmatrix}, \tag{31}$$

which is Eq. (9) in the main text. These matrix elements have the following explicit representations

$$\begin{aligned}
A^{xx}(\vec{k}) &= -\sum_{j=0}^{5} \mathcal{F}_j(\vec{k}) C_{ij}^{xx}(\phi) + \sum_{j=0}^{5} C_{ij}^{xx}(\phi), \\
A^{xy}(\vec{k}) &= -\sum_{j=0}^{5} \mathcal{F}_j(\vec{k}) C_{ij}^{xy}(\phi) + \sum_{j=0}^{5} C_{ij}^{xy}(\phi), \\
A^{yx}(\vec{k}) &= -\sum_{j=0}^{5} \mathcal{F}_j(\vec{k}) C_{ij}^{yx}(\phi) + \sum_{j=0}^{5} C_{ij}^{yx}(\phi), \\
A^{yy}(\vec{k}) &= -\sum_{j=0}^{5} \mathcal{F}_j(\vec{k}) C_{ij}^{yy}(\phi) + \sum_{j=0}^{5} C_{ij}^{yy}(\phi).
\end{aligned} \tag{32}$$

Similarly we have

$$\begin{aligned}
D^x(\vec{k}) &= -\sum_{j=0}^{5} \mathcal{F}_j(\vec{k}) C_{ij}^{x\sigma}(\phi) - \sum_{j=0}^{5} C_{ij}^{x\sigma}(\phi), \\
D^y(\vec{k}) &= -\sum_{j=0}^{5} \mathcal{F}_j(\vec{k}) C_{ij}^{y\sigma}(\phi) - \sum_{j=0}^{5} C_{ij}^{y\sigma}(\phi).
\end{aligned} \tag{33}$$

Inverting Eq. (31) leads to an expression for the Fourier transformed changes in positions in terms of the Fourier transformed changes in radii

$$\begin{aligned}
\delta x(\vec{k}) &= \alpha(\vec{k}) \delta\sigma(\vec{k}), \\
\delta y(\vec{k}) &= \beta(\vec{k}) \delta\sigma(\vec{k}),
\end{aligned} \tag{34}$$

which is Eq. (10) in the main text. Finally, an inverse Fourier transform and Eq. (29) yields the fluctuations in the positions at every site i

$$\begin{aligned}
\langle \delta x_i^2 \rangle &= \frac{1}{2L^2}\left(\frac{\eta^2}{48}\right)\sum_{m=0}^{L-1}\sum_{l=0}^{2L-1}(\alpha(\vec{k})\alpha(-\vec{k})),\\
\langle \delta y_i^2 \rangle &= \frac{1}{2L^2}\left(\frac{\eta^2}{48}\right)\sum_{m=0}^{L-1}\sum_{l=0}^{2L-1}(\beta(\vec{k})\beta(-\vec{k})),\\
\langle \delta x_i \delta y_i \rangle &= \frac{1}{2L^2}\left(\frac{\eta^2}{48}\right)\sum_{m=0}^{L-1}\sum_{l=0}^{2L-1}(\alpha(\vec{k})\beta(-\vec{k})).
\end{aligned} \tag{35}$$

Similarly, the fluctuations in the forces at every site i can be computed by expressing the linearized expressions in Eq. (21) in Fourier space. We have (with $j = 0$ to 5, see Fig. 3)

$$\begin{aligned}
\langle \delta f_{ij}^x \delta f_{ij}^x \rangle &= \frac{1}{2L^2}\left(\frac{\eta^2}{48}\right)\sum_{m=0}^{L-1}\sum_{l=0}^{2L-1}[C_{ij}^{xx}(1-\mathcal{F}_j(\vec{k}))\alpha(\vec{k}) + C_{ij}^{xy}(1-\mathcal{F}_j(\vec{k}))\beta(\vec{k}) + C_{ij}^{x\sigma}(1+\mathcal{F}_j(\vec{k}))]\\
&\times[C_{ij}^{xx}(1-\mathcal{F}_j(\vec{k})^{-1})\alpha(-\vec{k}) + C_{ij}^{xy}(1-\mathcal{F}_j(\vec{k})^{-1})\beta(-\vec{k}) + C_{ij}^{x\sigma}(1+\mathcal{F}_j(\vec{k})^{-1})],
\end{aligned} \tag{36}$$

$$\begin{aligned}
\langle \delta f_{ij}^y \delta f_{ij}^y \rangle &= \frac{1}{2L^2}\left(\frac{\eta^2}{48}\right)\sum_{m=0}^{L-1}\sum_{l=0}^{2L-1}[C_{ij}^{yx}(1-\mathcal{F}_j(\vec{k}))\alpha(\vec{k}) + C_{ij}^{yy}(1-\mathcal{F}_j(\vec{k}))\beta(\vec{k}) + C_{ij}^{y\sigma}(1+\mathcal{F}_j(\vec{k}))]\\
&\times[C_{ij}^{yx}(1-\mathcal{F}_j(\vec{k})^{-1})\alpha(-\vec{k}) + C_{ij}^{yy}(1-\mathcal{F}_j(\vec{k})^{-1})\beta(-\vec{k}) + C_{ij}^{y\sigma}(1+\mathcal{F}_j(\vec{k})^{-1})],
\end{aligned} \tag{37}$$

$$\begin{aligned}
\langle \delta f_{ij}^x \delta f_{ij}^y \rangle &= \frac{1}{2L^2}\left(\frac{\eta^2}{48}\right)\sum_{m=0}^{L-1}\sum_{l=0}^{2L-1}[C_{ij}^{xx}(1-\mathcal{F}_j(\vec{k}))\alpha(\vec{k}) + C_{ij}^{xy}(1-\mathcal{F}_j(\vec{k}))\beta(\vec{k}) + C_{ij}^{x\sigma}(1+\mathcal{F}_j(\vec{k}))]\\
&\times[C_{ij}^{yx}(1-\mathcal{F}_j(\vec{k})^{-1})\alpha(-\vec{k}) + C_{ij}^{yy}(1-\mathcal{F}_j(\vec{k})^{-1})\beta(-\vec{k}) + C_{ij}^{y\sigma}(1+\mathcal{F}_j(\vec{k})^{-1})].
\end{aligned} \tag{38}$$

In Fig. 5 we plot the variance in the components of the forces computed from numerical simulations at different polydispersities and packing fractions along with the above theoretical predictions. We find that the predictions from this theory match the simulations exactly at low η and begin to deviate at higher values of η where the higher order terms in the perturbation expansion begin to play a role.

Finally, we can also use the formalism developed here to compute the fluctuations in the bond angles $\sin\delta\theta_{ij}$ in the system. Once again expanding to linear order about the crystalline values, we have

$$\sin\delta\theta_{ij} = B_{ij}^x \delta x_{ij} + B_{ij}^y \delta y_{ij}, \tag{39}$$

where the coefficients are given by

$$\begin{aligned}
B_{ij}^x &= -\frac{\sin\theta_{ij}^0}{\sqrt{\phi_c/\phi}},\\
B_{ij}^y &= \frac{\cos\theta_{ij}^0}{\sqrt{\phi_c/\phi}}.
\end{aligned} \tag{40}$$

We then have

$$\begin{aligned}
\langle (\sin\delta\theta_{ij})^2 \rangle &= \frac{1}{2L^2}\left(\frac{\eta^2}{48}\right)\sum_{m=0}^{L-1}\sum_{l=0}^{2L-1}[B_{ij}^x(1-\mathcal{F}_j(\vec{k}))\alpha(\vec{k}) + B_{ij}^y(1-\mathcal{F}_j(\vec{k}))\beta(\vec{k})]\\
&\times[B_{ij}^x(1-\mathcal{F}_j(\vec{k})^{-1})\alpha(-\vec{k}) + B_{ij}^y(1-\mathcal{F}_j(\vec{k})^{-1})\beta(-\vec{k})].
\end{aligned} \tag{41}$$

The above expression along with the variance in the forces can then be used to compute the distribution of the orthogonal components of the forces $p(f_\perp)$ as described in the main text.

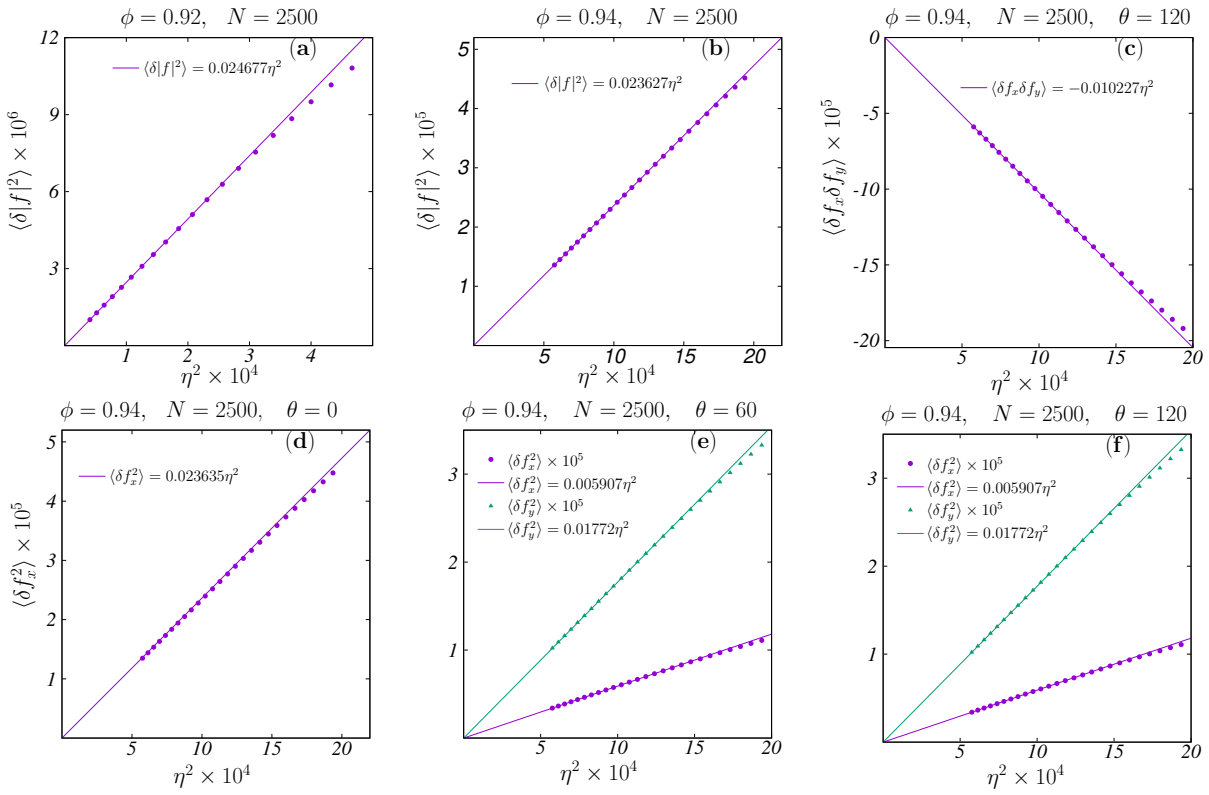

FIG. 5: Plot of the variance in the components of the forces computed from numerical simulations at different polydispersities (η) and packing fractions (ϕ) along with the theoretical predictions in Eqs. (36), (37) and (38). **(a)** Variance in the change in magnitude of the forces $\langle \delta|f|^2 \rangle$ for $\phi = 0.92$. **(b)** $\langle \delta|f|^2 \rangle$ for $\phi = 0.94$. These correlations have been computed by averaging over all six directions of the lattice ($j = 0$ to 5). **(c)** $\langle \delta f_x \delta f_y \rangle$ for $\phi = 0.94$ at an angle $\theta = 120$ ($j = 2$). **(d)** $\langle \delta f_x \delta f_x \rangle$ for $\phi = 0.94$ at $\theta = 0$ ($j = 0$). **(e)** $\langle \delta f_x \delta f_x \rangle$ and $\langle \delta f_y \delta f_y \rangle$ for $\phi = 0.94$, and $\theta = 60$ ($j = 1$). **(f)** $\langle \delta f_x^2 \rangle$ and $\langle \delta f_y^2 \rangle$ for $\phi = 0.94$ at $\theta = 120$ ($j = 2$). All quantities displayed have been computed for a system size $N = 2500$. We find that the predictions from the theory match the simulations exactly at low η and begin to deviate at higher values of η where the higher order terms in the perturbation expansion begin to play a role.

VIII. EXACT SERIES EXPRESSION FOR $p(f_\perp)$

Let x and y be two uncorrelated random variables The probability distribution of the variable $z = xy$ can then be expressed as

$$p(z) = \int_{-\infty}^{\infty} \int_{-\infty}^{\infty} p(x)p(y)\delta(z - xy)dxdy = \int_{-\infty}^{\infty} p(x)p\left(\frac{z}{x}\right)\frac{1}{|x|}dx. \tag{42}$$

Furthermore suppose x and y are normally distributed with means μ_1 and μ_2 and standard deviations σ_1 and σ_2 respectively. i.e.

$$p(x) = \frac{1}{\sqrt{2\pi\sigma_1^2}} e^{-\frac{(x-\mu_1)^2}{2\sigma_1^2}}, \tag{43}$$

and

$$p(y) = \frac{1}{\sqrt{2\pi\sigma_2^2}} e^{-\frac{(y-\mu_2)^2}{2\sigma_2^2}}. \tag{44}$$

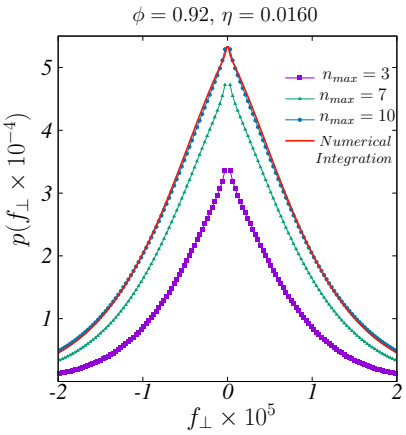

FIG. 6: Plot of the distribution of $f_\perp$ obtained from the exact series expression in Eq. (46) (with increasing number of terms n_{max}), along with a direct integration of the expression in Eq. (42). The two expressions converge as n_{max} is increased.

For such variables with non-zero means ($\mu_1 \neq 0, \mu_2 \neq 0$), the integral in Eq. (42) is non-trivial. However, it is still possible to obtain an exact series representation. The final expression of this integral has the following form [6]

$$p(z) = e^{-\left(\frac{\mu_1^2}{2\sigma_1^2}+\frac{\mu_2^2}{2\sigma_2^2}\right)} \sum_{n=0}^{\infty}\sum_{m=0}^{2n} \frac{z^{2n-m}|z|^{m-n}\sigma_1^{m-n-1}}{\pi(2n)!\sigma_2^{m-n+1}} \binom{2n}{m} \left(\frac{\mu_1}{\sigma_1^2}\right)^m \left(\frac{\mu_2}{\sigma_2^2}\right)^{2n-m} K_{m-n}\left(\frac{|z|}{\sigma_1\sigma_2}\right). \tag{45}$$

Here $K_{m-n}(.)$ is the modified Bessel function of the second kind of order $(m-n)$. This function displays non-analytic behaviour at $z = 0$. The case we are considering $f_\perp = |f|\sin(\delta\theta)$ has $\langle \sin(\delta\theta)\rangle = 0$, and $\langle |f|\rangle = f_0 \neq 0$. The final expression of this integral can be simplified to the following form

$$p(f_\perp) = e^{-\left(\frac{f_0^2}{2\sigma_1^2}\right)} \sum_{n=0}^{\infty} \frac{|f_\perp|^n \sigma_1^{n-1}}{\pi(2n)!\sigma_2^{n+1}} \left(\frac{f_0}{\sigma_1^2}\right)^{2n} K_n\left(\frac{|f_\perp|}{\sigma_1\sigma_2}\right), \tag{46}$$

where σ_1 and σ_2 are the standard deviations of the fluctuations in the forces $|f|$ and $\sin(\delta\theta)$ respectively, which we have computed in Eqs. (36 – 38) and Eq. (41). In Fig. 6 we plot the distribution of $f_\perp$ obtained from the above series (with an increasing number of terms), and a direct integration of the expression in Eq. (42), showing the convergence of the above exact series expression to the numerically integrated curve displayed in Fig. 3 in the main text.

IX. JOINT DISTRIBUTION OF $|f|$ AND $\sin(\delta\theta)$

In this Section we analyze the correlations between the variables $|f|$ and $\sin(\delta\theta)$ which we use to compute the distribution of $f_\perp = |f|\sin(\delta\theta)$.

As we show in the main text, the force balance conditions on every particle yield $2N$ equations for the $2N$ position variables $\{x_i, y_i\}$. Since this system of equations is invertible, these position variables are linearly independent. The forces, and the relative bond angles then be derived from these positions by linearizing the force law. As the forces are derived from the bond distances, not all the forces in the system are independent. In the triangular lattice arrangement, there are $N_C = 6N_G$ *vector* bond variables (f_{ij}^x and f_{ij}^y), where N_C is the total number of contacts, and N_G is the number of particles in the system. However, since $\vec{f}_{ij} = -\vec{f}_{ji}$, these reduce to $3N_G$ vector variables. Clearly, the representation of the degrees of freedom in the system in terms of the forces then is an overparametrization. There are therefore additional constraints that these variables must satisfy. It is easy to see that these are the loop constraints providing $2N_G$ vector equations, leaving the system with N_G independent vector variables.

In the derivation of the distribution of $f_\perp$, we have assumed that the parametrization of the system in terms of the magnitude of each force $|f_{ij}|$ and the relative angles measured in terms of the original lattice directions $\delta\theta_{ij} = \theta_{ij} - \theta_{ij}^0$. This is in effect a $\{f_{ij}^x, f_{ij}^y\} \to \{|f_{ij}|, \delta\theta_{ij}\}$ transformation. Therefore the loop constraints still need to be imposed on these variables. However, these are higher order correlations as we show below. In our linear theory, we can compute

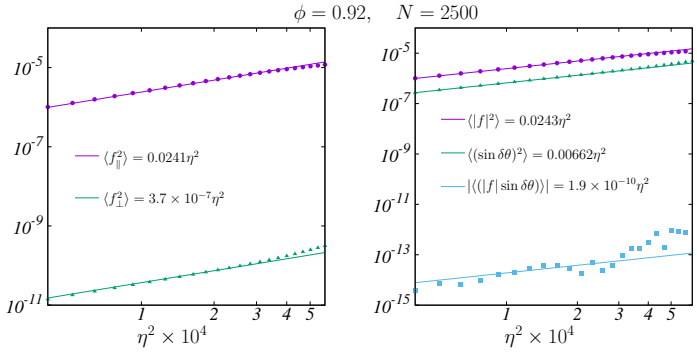

FIG. 7: (Left) Plot of the variance in the components of the forces, showing that the fluctuations in $f_\perp$ are much smaller than the fluctuations in $f_{||}$. (Right) The correlation between $|f_{ij}|$ and $\sin \delta\theta_{ij}$ is much smaller in comparision to their individual fluctuations.

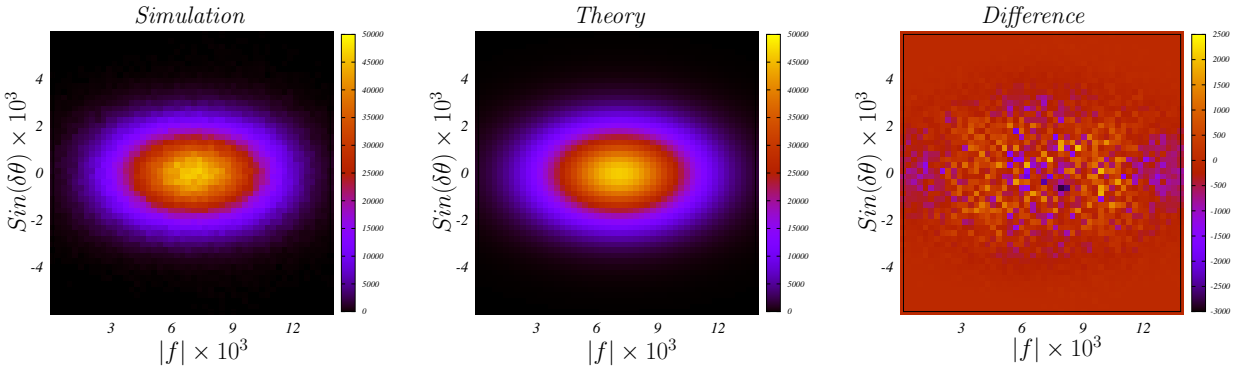

FIG. 8: The joint distribution of the variables $|f|$ and $\sin \delta\theta$, observed in the numerics (left) and using an uncorrelated form predicted from the linear theory (middle). The (right) panel displays the difference between these two distributions, showing that to leading order this distribution can be reproduced using the marginal distributions of each of these variables.

the correlations in these variables to leading order exactly. We find

$$\begin{aligned} \langle |f|^2 \rangle &= 0.0241\eta^2, \\ \langle \sin^2 \delta\theta \rangle &= 6.62 \times 10^{-3}\eta^2. \end{aligned} \tag{47}$$

However, as our linear theory predicts that the correlation $\langle |f| \sin \delta\theta \rangle$ is exactly zero to lowest order, we have also measured the following correlation in our simulations and find

$$|\langle |f| \sin \delta\theta \rangle| = 1.9 \times 10^{-10}\eta^2. \tag{48}$$

Therefore, to leading order the cross-correlations between these variables is very small in comparison to their individual fluctuations, justifying our uncorrelated computation. In Fig. 7 we plot the variance in the components of the forces, as well as the above correlations. Taking the uncorrelated assumption further, the joint distribution of the variables $|f|$ and $\sin \delta\theta$ can be written as a product form

$$p(|f|, \sin \delta\theta) = p(|f|)p(\sin \delta\theta). \tag{49}$$

In Fig. 8 we plot the joint distribution of the variables $|f|$ and $\sin \delta\theta$ obtained from simulations, as well as from the above uncorrelated product form, showing that to leading order this distribution can be reproduced using the marginal distributions of each of these variables.

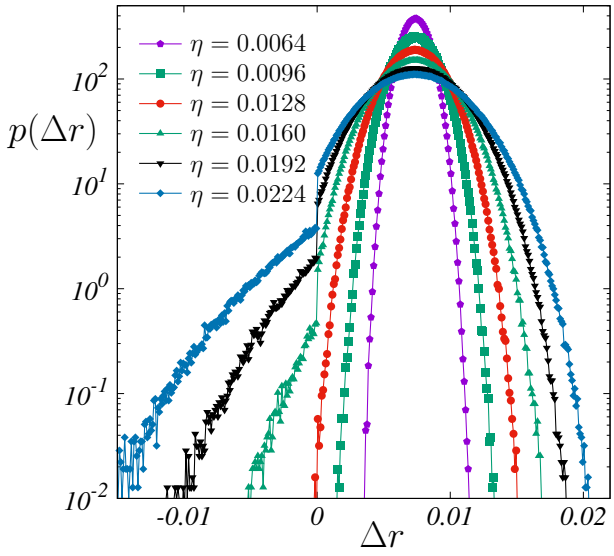

FIG. 9: Distribution of overlap lengths $\Delta r_{ij} = \sigma_i + \sigma_j - |\vec{r}_i - \vec{r}_j|$ between particles at different polydispersities (η) for $\phi = 0.92$. For low polydispersities all overlaps are positive, i.e. there are no broken contacts. At higher η, contacts break and the overlap distribution develops a discontinuity, signifying system spanning rearrangements.

X. DISTRIBUTION OF OVERLAP LENGTHS

Finally, we investigate the origin of the small deviation in the average coordination predicted by the theory and those obtained from numerical simulations as shown in Fig. 4 in the main text. To study the process of contact breaking in the system, we analyze the distribution of overlap lengths $\Delta r_{ij} = \sigma_i + \sigma_j - |\vec{r}_i - \vec{r}_j|$ between neighbouring particles i and j in the system. $\Delta r > 0$ represent real (force bearing) contacts, whereas $\Delta r < 0$ represent the broken contacts in the system. Since we have focused on harmonic interactions in this study, the distribution $p(\Delta r)$ for $\Delta r > 0$ is exactly the distribution of forces $p(|f|)$ (with a suitable normalization). As the crystalline systems we study have $\Delta\phi > 0$, all the contacts bear a finite force and $\Delta r > 0$ at $\eta = 0$, with $p(\Delta r) = \delta(\Delta r - f_0)$ (as given in Eq. (12)). With increasing polydispersity, this distribution broadens and contacts begin to break, populating the $\Delta r < 0$ regions. We plot this distribution for different polydispersities in Fig. 9. Surprisingly, although both regions are well fit by Gaussians, they are separated by a discontinuity. This suggests that as a bond between two particles breaks, Δr moves a finite distance away from 0. We have tested that this is indeed the case by gradually increasing the polydispersity and following the evolution of the broken contacts in the system. We attribute this "kick" felt by these bonds as originating from the system spanning rearrangements that occur in response to a contact breaking event. As our prediction for z in Eq. (13) in the main text was obtained from the distribution of the force magnitudes extrapolated to the unphysical regions $|f| < 0$, the finite discontinuity in the Δr distribution explains the origin of the shift in the numerically obtained z and those predicted by the theory. It would be interesting to extend our methods to develop an explanation for this non-linear contact breaking process.

[1] R. C. Ball and R. Blumenfeld, Physical review letters **88**, 115505 (2002).
[2] K. Ramola and B. Chakraborty, Journal of Statistical Physics **169**, 1 (2017).
[3] E. Bitzek, P. Koskinen, F. Gähler, M. Moseler, and P. Gumbsch, Physical review letters **97**, 170201 (2006).
[4] H. Tong, P. Tan, and N. Xu, Scientific reports **5**, 15378 (2015).
[5] T. Horiguchi, Journal of Mathematical Physics **13**, 1411 (1972).
[6] G. Cui, X. Yu, S. Iommelli, and L. Kong, IEEE Signal Processing Letters **23**, 1662 (2016).